Borneo Engineering & Advanced Multidisciplinary International Journal (BEAM)
Volume 4, Special Issue (TECHON 2025), September 2025, Pages 56-64

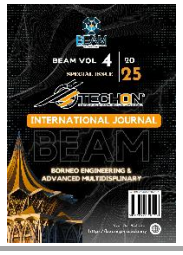

Optimization of Turbofan Engine Nacelles Design for Boeing 777X by Using Computational Fluid Dynamic Analysis

Nova Zena Vania[1]*, Andrew Ragai Henry Rigit[1]

[1]Department of Mechanical Engineering, Universiti Malaysia Sarawak, Jalan Datuk Mohammad Musa, 94300 Kota Samarahan, Sarawak, Malaysia

*Corresponding author: novazenav@gmail.com
Please provide an **official organisation email** of the corresponding author

Full Paper

Article history
Received
28 June 2025
Received in revised form
10 July 2025
Accepted
19 August 2025
Published online
30 September 2025

Abstract

The efficient design of turbofan engine nacelles is critical for enhancing aircraft performance and supporting sustainable aviation goals. This study investigates the aerodynamic and thermal performance of various nacelle configurations for the Boeing 777X GE9X engine, focusing on innovative cooling strategies and drag reduction. By Using Computational Fluid Dynamics (CFD) simulations, nacelle shapes of varying lengths (10 m and 5.5 m), including long and short nacelles with and without chevrons, as well as an optimized ultra-short nacelle, were analyzed under cruise conditions. Models were developed using MATLAB and SolidWorks, and simulations were performed in ANSYS Fluent. Results indicate that the long nacelle with chevrons provided the best overall thermal and aerodynamic performance among the conventional designs, reducing drag and block fuel consumption by 10.13%. However, the optimized ultra-short nacelle, developed using a hybrid NSGA-II and fmincon optimization approach by using MATLAB, achieved a significantly lower drag coefficient and reduced block fuel consumption by 80.13%. These findings demonstrate the potential of advanced nacelle designs to improve heat dissipation, reduce aerodynamic drag, and lower emissions, aligning with stringent EASA standards and contributing to sustainable aviation advancements.

Keywords: - Engine Nacelle Design, Boeing 777X, computational Fluid Dynamics (CFD), turbofan

1. Introduction

Aviation has consistently driven innovation, with each aircraft component optimized for performance, safety, and sustainability. The engine nacelle, a streamlined structure housing the engine, plays a vital role in aerodynamic efficiency, noise reduction, and protection against external hazards such as debris and lightning. However, modern nacelle design faces growing challenges, particularly in thermal management. Elevated engine temperatures and nacelle-induced pressure losses can increase fuel consumption and emissions. For instance, a 1% bypass duct pressure loss can raise fuel use by 2% (Nikolaidis et al., 2020). Additionally, climate change has intensified phenomena like clear-air turbulence (CAT), further impacting safety, fuel efficiency, and operational costs (Prosser et al., 2023 & Foudad et al., 2022). These factors underscore the urgent need for innovative nacelle designs capable of addressing both thermal and environmental challenges.

2. Literature Review

Designing a nacelle for an engine involves addressing challenges related to achieving optimal aerodynamic efficiency, maintaining structural integrity, and ensuring environmental sustainability. To tackle these challenges, a comprehensive approach is essential, combining innovative nacelle designs with advanced computational techniques, including Computational Fluid Dynamics (CFD). A redesigned engine nacelle can significantly enhance the efficiency of turbofan engines while

simultaneously reducing operating temperatures and emissions. Modifications to the shape and length of existing nacelles are integral to these improvements. In this study, Equations of class shape transformation and fuel efficiency will be employed to facilitate the design and optimization of the nacelle. Compliance with aviation standards, such as EASA CS-25.1191 (Firewall), EASA CS-25.1091 (Cooling Efficiency), EASA CS-E 800 (Bird Strike Energy), Pressure Recovery (IPR)/Airflow Efficiency, Aerodynamic Drag (Nacelle Drag Coefficient) will ensure structural and safety integrity throughout the design process.

Recent challenges faced by the Boeing 777X highlight the critical need for innovative nacelle designs. Issues with fuel consumption and efficiency stem from high thrust requirements, which increase fuel burn during critical flight phases. Inefficiencies in predictive modelling further exacerbate this problem, with studies revealing a mean underestimation of fuel use by 3 tons across diverse flight profiles (Schuster & Haag, 2022). Additionally, high operating temperatures, a by-product of increased thermal efficiency, impose significant stress on engine components, necessitating advanced thermal management systems (Edwards, 2000 & Fischer, 2006). These challenges underscore the need for nacelles that not only improve aerodynamic performance but also effectively manage heat and reduce drag. Chevron nozzles are a critical feature in modern nacelle designs for aircraft engines whereby it can improve nacelle pressure distribution, contribute to more uniform temperature gradients, and significantly reduce drag coefficients.

3. Methodology

This study employs quantitative and simulation methods to optimize nacelle designs for the Boeing 777X by varying shape and length to minimize engine temperature, fuel consumption, and emissions.

3.1 Procedure for Objective 1 and 2

The nacelles designs will be created in Autodesk SolidWorks. However, before imported into Autodesk SolidWorks, the trailing edge is produced by using MATLAB.

3.1.1 Design Procedure

There are several step producing engine nacelles designs such as:

Step 1: Class Shape Transformation (CST)

$$\text{Base Shape Function, } B(\psi) = l_{nac} + \psi(r_{te} - r_{hi}) \quad (1)$$

$$Point, \psi = \frac{x}{l_{nac}}$$

$$\text{Class Function , } C(\psi) = \psi^a(1-\psi)^b$$

a = leading edge (m)

b= *trailing edge* (m)

$$\textit{Shape Function}, S(\psi) = \sum_{i=0}^{n} bc_i\, \psi^i\, (1-\psi)^{n-1}.\, A_i \quad (2)$$

$$\sum_{i=0}^{n} \frac{n!}{i!\ .\ (n-i)!}$$

$$A_i = Coefficient\ that\ define\ the\ contribution\ of\ each\ term\ to\ the\ shape$$

n = Degree of Bernstein polynomial (control the number of terms in the expansion)

$$\textit{Complete Shape Function}, y(x) = B(\psi) + C(\psi) + S(\psi) \quad (3)$$

$$Mass - flow\ Capture\ Ratios, MFCR \frac{A_c}{A_f} \quad (4)$$

Step 2: Choosing EASA number for the shape of the nacelle

Table 1: Design parameter of engine nacelle

Parameter	Values		Description
r_{hi}	1.3194 m		Highlight radius
r_{te}	1.20197 m		Trailing edgement
l_{nac}	10m	5.5m	Nacelle length
r_{if}	0.12526 m		Initial fore body radius
β	11°		Boat tail angle
d_i	2.423 m		Inlet diameter
d_m	2.85 m		Maximum diameter
d_e	2.40394 m		Exit diameter

Based on the class shape transformation (CST) in step 1, the shape of trailing edge of the nacelle design is formed for both shape by using Matlab as shown in Fig. 1.

The trailing edge retrieved from Matlab is used as the guideline to generate the full shape of nacelle. This form of the nacelle will be imported into Autodesk SolidWorks to refine the shape by using revolved Boss/Base command. There are 2 types of the nacelle which as 10 m and 5.5 m length, and with/out chevron nacelle as shown in Fig. 2.

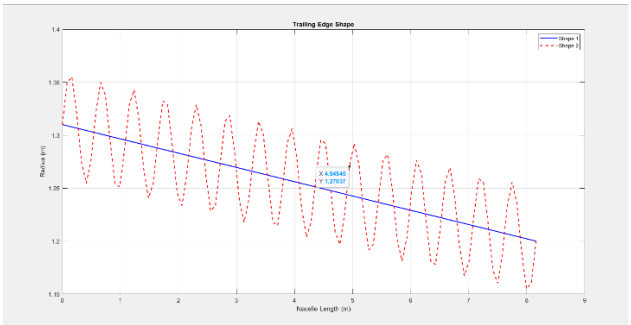

Fig. 1: Trailing edge shape from MATLAB

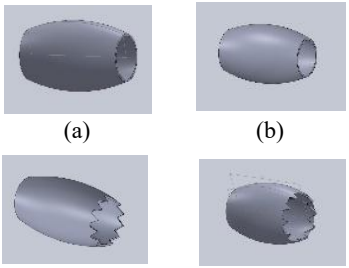

(a) (b)

(c) (d)

Fig.2: Non-axisymmetric engine nacelle (a) Long Shape Without Chevron, (b) Short Nacelle Without Chevron, (c) Long Nacelle with Chevron and (d) Short Nacelle with Chevron

3.1.2 Simulation Procedure

After the model stage is completed, the next step is simulation of the model by using Ansys Fluent. In this case, the objective of the simulation is to analyse aerodynamic drag, heat dissipation, and engine efficiency. The nacelles design models are drawn to scale based on measurements provided by researchers to enhance accuracy and precision. However, due to limited access to the original data, the author will estimate some values for simulation. The simulation is assumed in steady-state flow. The simulation process comprises three phases: pre-processing, numerical solution, and post-processing. The flow of simulation of nacelle design is shown in Fig. 3.

Table 2: Meshing settings for all engines Nacelles models

Element Order	Adjustment
Element Size	664 mm
Smoothing	High
Mesh Metric	Skewness
Triangle Surface Mesher	Advancing Front

Table 3: Parameters for CFD solver in ANSYS Fluent

Solver	• Type: Density-based • Velocity formulation: Absolute • Time: Steady
Model	• Energy: On • Viscous: SST k-omega (2 eqn)
Fluid Materials	• Air • Density: Ideal-gas • Viscosity: Sutherland
Boundary Conditions	**For temperature and pressure** • Inlet: Pressure Inlet • Gauge Total Pressure: 25000 Pa, 40000 Pa • Supersonic/Initial Gauge Pressure: 94500 • Thermal: 973.15K, 288.15 • Wall: Stationary wall, No Slip • Outlet: Pressure outlet • Gauge pressure outlet 15000 Pa, 34300 Pa **For drag coefficient** • Inlet: Velocity-Inlet • Velocity Magnitude: 250.81 m/s • Supersonic/Initial Gauge Pressure: 94500 Pa • Thermal 973.15 K • Outlet: Pressure Outlet • Gauge pressure outlet: 15000 Pa
Reference Value	• Compute from: Inlet • Velocity: 250.81 m/s
Solution Methods	• Formulation: Implicit • Flux type: Roe-FDS • Gradient: Least squares cell based • Flow: Second Order Upwind • Turbulent Kinetic Energy: Second Order upwind • Specific Dissipation Rate: Second Order Upwind
Solution Initialization	• Standard Initialization • Compute from: inlet • Reference frame: relative to cell zone
Run Calculation	• Number of Iterations: 1000 • Reporting Interval: 1 • Profile Update Interval: 1

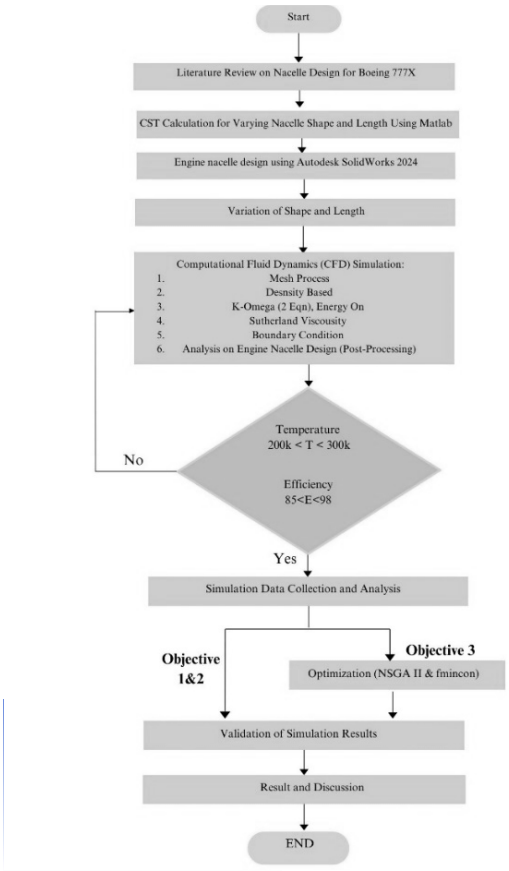

Fig. 3: Flow chart of the research methodology

After completing the simulations, the aerodynamic drag of the nacelle is obtained, which allows the determination of engine efficiency. The thrust generated by the engine is identified. The fuel efficiency due to each nacelle can be determined by using this equation (5).

$$\mathrm{D} = \frac{1}{2}\rho V^2 S C_d \quad (5)$$

$$\rho = Density\ of\ the\ air\ (kg/m^2$$

$$V = Velocity\ (\frac{m}{s})$$

$$S = Wing\ Area\ (427.35\ m^2)$$

$$C_d = Drag\ Coefficient$$

Once the nacelle drag is calculated, the fuel flow can be determined equation (6).

$$Fuel\ Flow = D \times TSFC \quad (6)$$

$$D = Drag$$

$$TSFC = Thrust\ Specific\ Fuel\ Consumption$$

After calculating the required fuel flow, the block fuel can be determined using the equation (7).

$$Block\ Fuel = Fuel\ Flow \times Time \quad (7)$$

$$\text{Time} = \frac{3000}{488}$$

$$= 6.15\ hours\ (\text{time to fly 3000 nmi})$$

Finally, engine efficiency can be evaluated using the appropriate efficiency formula.

$$\text{Percent Change} = \left(\frac{Block\ Fuel - Baseline\ Block\ Fuel}{Baseline\ Block\ Fuel}\right) \times 100\% \quad (8)$$

After obtaining the percentage changes or engines efficiency, the result is compared to others researcher results which are from Nasa data.

3.2 Procedure for Objective 3

To achieve an optimized ultra-short nacelle configuration, a hybrid optimization approach combining NSGA-II and fmincon was employed. The initial geometry was based on earlier objectives and refined using SolidWorks, with the trailing edge profile generated via equations (1) until (4). The final design integrated features from both short nacelles and modified chevrons, as illustrated in Fig. 5. Computational simulations were conducted under consistent conditions (see Table 3), and fuel efficiency was assessed using equations (5) until (8). This optimization aimed to reduce drag, enhance temperature distribution, improve fuel efficiency, and produce an aerodynamically efficient trailing edge.

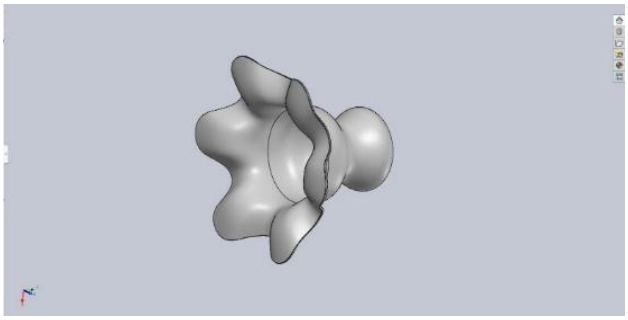

Fig. 5: Model for optimized ultra-short Nacelle design

4. Result and Discussion

The results are obtained through simulation conducted at a velocity of 250.81 m/s, an altitude of 11, 278 meters, and an angle of attack of 0º, representing the cruise condition of a Boeing 777X**.**

4.1 Temperature Results of Four Nacelles

The results highlight the critical influence of nacelle geometry on thermal behaviour under cruise conditions as shown in Fig. 7. Tomita et al. (2005) reported a 217 K temperature for a 7 m nacelle, serving as a benchmark. In contrast, the short nacelle without chevrons (5.5 m) reaches 287.9 K (circle marker), significantly higher due to limited duct length, which restricts flow deceleration and thermal dissipation. The addition of chevrons to this short nacelle further increases the temperature to 295 K (rectangle marker), indicating that chevron-induced turbulence and vortex mixing while beneficial for noise reduction and flow control (Wernet & Bridges, 2021 & Jawahar et al., 2022) can generate localized heating when insufficient downstream length is available for dissipation. The long nacelle without chevrons (10 m) registers a reduced temperature of 238 K (diamond marker), slightly above Tomita's case, due to enhanced flow diffusion and passive cooling over the extended duct. Notably, the long nacelle with chevrons achieves the lowest observed temperature of 200 K (pentagon marker), demonstrating that chevrons significantly improve thermal performance when coupled with a sufficiently long nacelle. This configuration allows turbulent mixing to occur within the duct length, promoting uniform flow and more effective heat dispersion, aligning with findings in (Tejero et al., 2019 & General Electric Company, 2023).

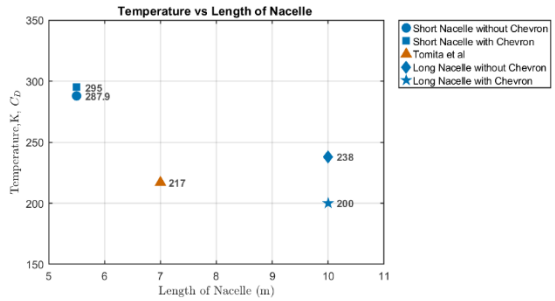

Fig.6: Comparison of temperature obtained for each nacelle shape from current simulation with other researcher

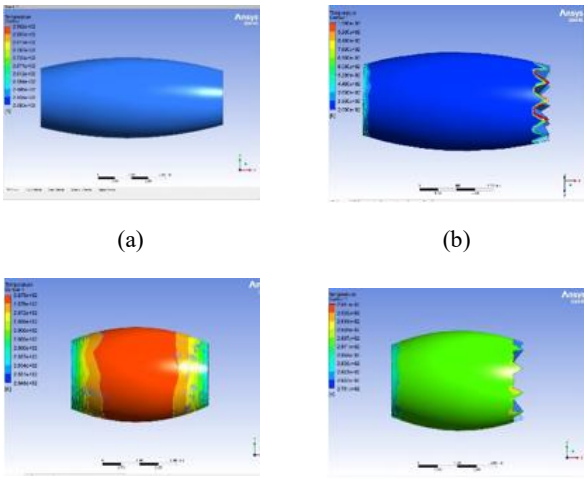

(a) (b)

(c) (d)

Fig. 7: Comparison of the temperature of turbofan engine Nacelle designs (a) long shape without Chevron, (b) short Nacelle without Chevron, (c) long nacelle with Chevron and (d) short nacelle with Chevron

4.2 Pressure Results of Four Nacelles

Fig. 9 compares the simulated pressure distributions of various nacelle configurations with those reported in previous studies. The results emphasize the significant impact of nacelle length and geometry particularly the presence of chevrons on static pressure behaviour along the nacelle surface.

In general, longer nacelles result in lower overall pressure due to smoother flow deceleration and enhanced pressure recovery. The configuration by Tomita et al. (2005), indicated by a triangular marker, reported the lowest pressure at 22,200 Pa, reflecting highly efficient flow management. In contrast, the short nacelle without chevrons (circular marker) exhibited the highest pressure at 38,910 Pa due to abrupt boundary layer deceleration and limited surface area for pressure diffusion.

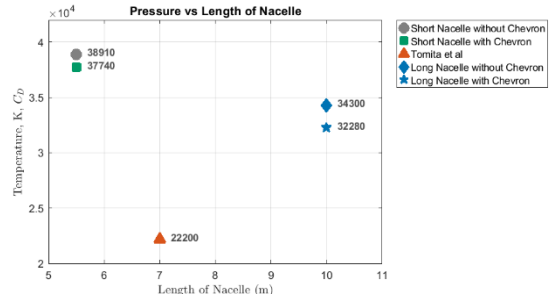

Fig. 8: Comparison of pressure obtained for each nacelle shape from current simulation with other researcher

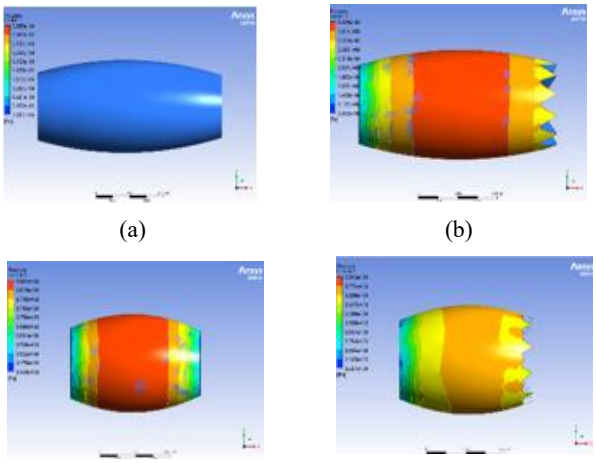

(a) (b)

(c) (d)

Fig. 9: Comparison of the pressure of turbofan engine nacelle designs (a) long shape without Chevron, (b) short nacelle without Chevron, (c) long nacelle with Chevron and (d) short nacelle with Chevron

The introduction of chevrons, designed to improve shear-layer mixing and mitigate flow separation, demonstrated measurable benefits. The short nacelle with chevron (rectangular marker) showed a reduced pressure of 37,740 Pa, while the long nacelle with chevron recorded the lowest pressure among the current designs at 32,280 Pa. This reduction is attributed to the chevrons generating streamwise vortices that enhance ambient air entrainment and reduce wake pressure, consistent with findings by Wernet & Bridges (2021) & Tam & Parrish (2008).

Although all tested configurations showed higher pressures than the Tomita et al. (2005), the long nacelle with chevrons proved to be the most aerodynamically effective among the present designs. This highlights the synergistic benefit of combining extended nacelle length with chevron-induced vortex structures to enhance pressure recovery and overall flow control.

4.3 Drag Coefficient Results of Four Nacelles

Fig. 11 presents a comparative analysis of the drag coefficients obtained from the current Computational Fluid Dynamics (CFD) simulations against the experimental findings of Frede and Takashi under cruise conditions. The configuration studied by Frede and Takashi, denoted by a triangle marker in Fig. 4.20, recorded a drag coefficient (C_d) of 0.058. In contrast, the short nacelle without chevrons yielded a higher drag coefficient of 0.099 (circular marker), while the short nacelle with chevrons produced the highest drag coefficient among all tested configurations at 0.278.

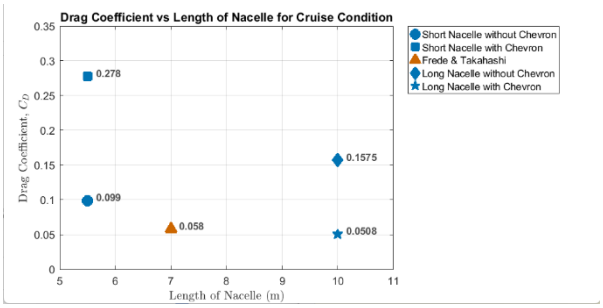

Fig. 10: Comparison of drag coefficient obtained for each nacelle shape from current simulation with other researcher

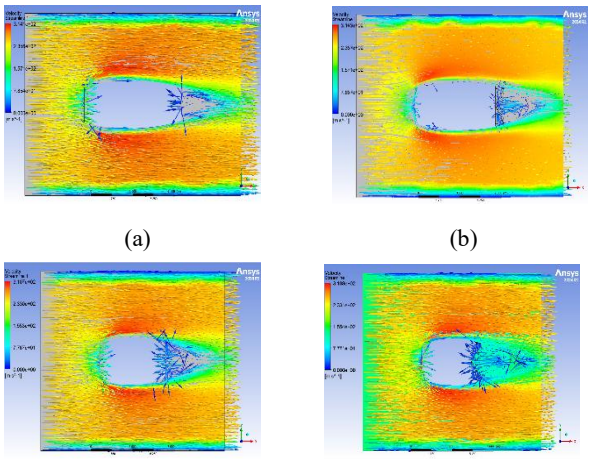

Fig. 11: Comparison of the airflow of turbofan engine nacelle designs (a) long shape without Chevron, (b) short nacelle without Chevron, (c) long nacelle with Chevron and (d) short nacelle with Chevron

The observed differences in drag performance are largely attributed to variations in nacelle length and the presence of chevron structures. Specifically, the long nacelle without chevrons achieved a drag coefficient of 0.1575 (parallelogram marker), suggesting improved flow development over the shorter designs, but still exhibiting considerable wake formation.

In contrast, the long nacelle with chevrons achieved the lowest drag coefficient of 0.0508 (pentagon marker), slightly outperforming the Frede and Takashi configuration. This enhanced aerodynamic behaviour is primarily due to the synergistic effects of extended nacelle length and chevron-induced flow control. The chevrons, which are serrated structures at the trailing edge, generate streamwise vortices that enhance shear layer mixing and reduce turbulence intensity at the nozzle exit (Daggett et al., 2003 & Wernet & Bridges, 2021). These controlled vortices help delay boundary layer separation, suppress recirculating flow regions, and reduce adverse pressure gradients. As a result, the wake is more organized and narrower, leading to a significant reduction in pressure (form) drag.

Moreover, chevrons contribute to improved flow symmetry and velocity reattachment at the nacelle aft-body, promoting smoother flow detachment and improved pressure recovery. The long nacelle provides sufficient surface length for gradual velocity development and supports laminar-to-turbulent transition without premature separation. When combined, the extended nacelle geometry and chevron features yield a stable, high-momentum wake with reduced turbulence and lower drag, as validated by the minimum drag coefficient observed in this study.

4.4 Fuel Efficiency Results for Four Nacelles

Fig. 12 shows the correlation between drag coefficient and block fuel consumption for different nacelle configurations. The long nacelle with chevrons achieved the best performance, reducing fuel usage by 10.13%, slightly outperforming NASA's UEET reference configuration at –10.00%. This improvement is attributed to the chevron's ability to enhance jet mixing, reduce shear-layer separation, and improve pressure recovery, leading to lower aerodynamic drag (Daggett et al., 2003 & Wernet & Bridges, 2021).

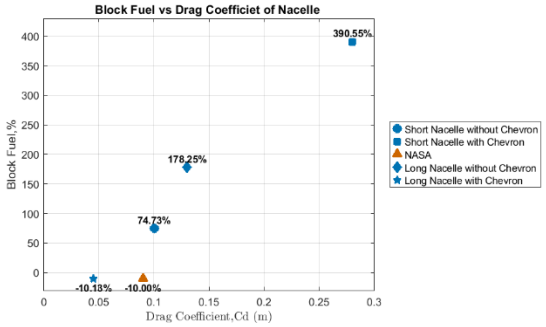

Fig. 12: Comparison of block fuel obtained for each nacelle shape from current simulation with other researcher

In contrast, the short nacelle with chevrons showed the highest fuel consumption (+390.55%), followed by the long nacelle without chevrons (+178.25%) and the short nacelle without chevrons (+74.73%). These results emphasize that nacelle length alone does not ensure fuel

efficiency effective flow control features like chevrons are essential.

The performance aligns with NASA's UEET findings, which highlighted the benefits of optimized BPR, advanced shaping, and nacelle integration. The chevron-enhanced long nacelle replicates these aerodynamic principles, achieving superior fuel efficiency through reduced drag and improved flow control.

4.5 Optimized Ultra-short Nacelle

Fig. 14 shows that the optimized ultrashort nacelle exhibits a higher surface temperature (280 K) than the configuration by Robinson et al. (2020) (273.15 K), due to its compact geometry, which may induce flow separation and reduce cooling efficiency. As noted by Tejero et al. (2019), non-monotonic curvature, particularly near the afterbody and trailing edge, can lead to localized heat accumulation. A key factor in thermal performance is the chevron geometry at the trailing edge. The broader chevron on the optimized nacelle enhances core-bypass mixing, promoting early thermal dissipation and reducing downstream eddies. This results in a lower temperature than short nacelles without chevrons (295 K) and with chevrons (287.9 K). While long nacelles show the lowest temperatures (238 K and 200 K) due to extended flow development, the ultrashort nacelle's chevron compensates by improving thermal mixing, consistent with findings by Wernet & Bridges (2021) on vortex breakdown and thermal spreading.

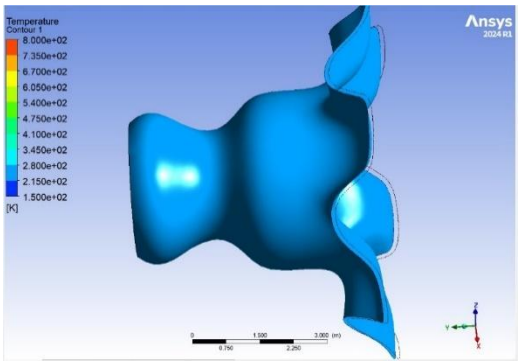

Fig. 13: Temperature distribution for ultra-short nacelle

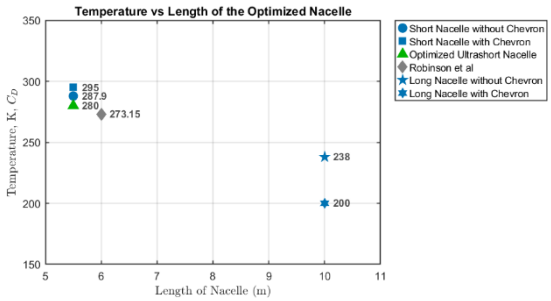

Fig. 14: Comparison of temperature obtained for ultra-short nacelle from current simulation with Robinson et al. (2020)

Fig. 15 shows the pressure distribution on the optimized ultra-short nacelle, where the dark blue contour indicates a uniform low pressure of 26,250 Pa near the trailing edge, attributed to the broader chevron geometry. This design enhances jet and ambient air mixing, reducing turbulence and vortex formation as noted by Wernet & Bridges (2021). A pressure rise at the midsection results from sharp curvature causing a recirculation zone that increases local static pressure and lowers aerodynamic efficiency. Elevated pressure near the trailing edge stems from turbulent wake interactions and vortex shedding, which the chevron helps mitigate through smoother mixing.

Fig. 16 compares nacelle pressures, showing the optimized ultra-short nacelle achieves the lowest pressure (26,250 Pa) versus Robinson et al. (2020) 41,000 Pa and other designs. The chevron's vortex disruption and enhanced mixing reduce drag and improve aerodynamic performance.

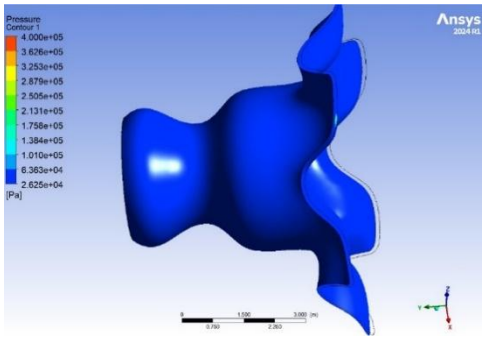

Fig. 15: Pressure distribution for ultra-short nacelle

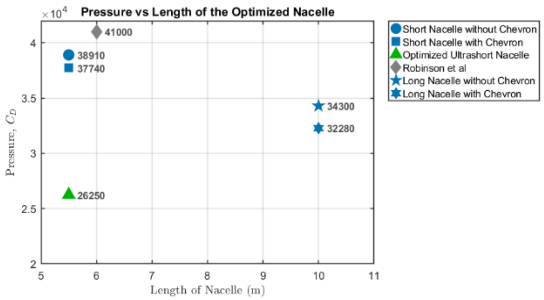

Fig. 16: Comparison of pressure obtained for ultra-short nacelle from current simulation with Robinson et al. (2020)

Fig. 17 shows the airflow distribution around the ultra-short nacelle, highlighting smooth flow attachment and minimal separation at the inlet and trailing edges, which reduces drag. With a length-to-diameter ratio of 0.35, this nacelle is more compact than traditional designs, reducing wetted area and drag CD=0.0248, compliant with EASA standards (European Union Aviation Safety Agency, 2020a & Silva et al., 2022). The trailing edge features chevrons that smooth curvature transitions, minimizing flow separation and boundary layer distortion (Tejero et al., 2019).

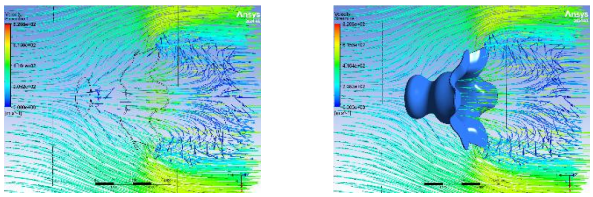

(a) (b)

Fig. 17: Drag coefficient result for optimized ultra-short nacelle (a) airflow of ultra-short nacelle and (b) airflow exit from ultra-short nacelle

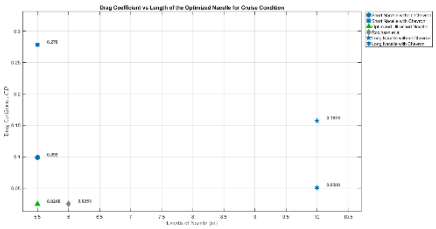

Fig. 18: Comparison of drag coefficient for cruise condition: ultra-short nacelle (current simulation vs. Robinson et al. (2020))

At the inlet, flow recirculation and vortices arise due to sharp curvature causing adverse pressure gradients and boundary layer separation, as seen in Fig. 18. Conversely, the trailing edge shows outward flow, indicating effective wake management and pressure recovery. The use of Class Shape Transformation (CST) enables precise curvature control, maintaining flow attachment and reducing vortex formation (Jawahar et al., 2022 & Millot et al., 2019). Fig. 19 compares drag coefficients under cruise conditions, with the optimized ultra-short nacelle achieving CD=0.0248, outperforming Robinson et al. (2020) CD=0.0253. The broader trailing edge with chevrons stabilizes the wake, lowers base drag, and supports thermal exhaust integration without compromising aerodynamics (European Union Aviation Safety Agency, 2020b & Tejero et al., 2019). These results confirm that geometric optimization, especially at the trailing edge, significantly improves aerodynamic efficiency.

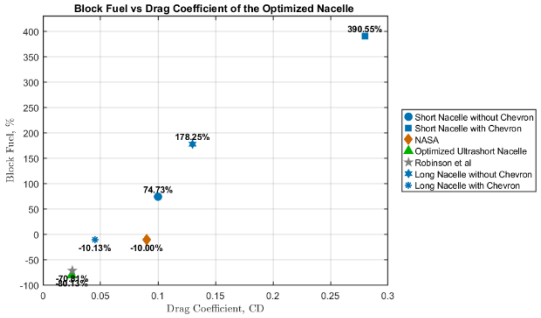

Fig. 19: Comparison of drag coefficient for cruise condition: ultra-short nacelle (current simulation vs. Robinson et al. (2020))

The optimized ultra-short nacelle achieves a significant block fuel reduction of 80.13%, outperforming Robinson et al. (2020) configuration at 78.81% and far exceeding NASA's 10.00% reduction as shown by Fig. 19. This improvement reflects superior aerodynamic efficiency achieved by minimizing drag (CD=0.0248) and optimizing the nacelle's length-to-diameter ratio (L/D) and fan pressure ratio (FPR), as well as integration with the airframe.

The NASA study highlights reducing wave and profile drag by refining L/D to prevent shock formation. The optimized nacelle's shorter length and expanded trailing-edge chevrons promote even airflow distribution, reducing drag and enhancing fuel economy in compliance with EASA standards. In contrast, configurations such as Short Nacelle with Chevron (+390.55%) and Long Nacelle without Chevron (+178.25%) show large increases in block fuel consumption due to aerodynamic inefficiencies and higher wetted areas.

5. Conclusion and Recommendations

This study investigates the aerodynamic and thermal performance of various nacelle configurations for the Boeing 777X under cruise conditions, focusing on long and short nacelles with and without chevrons and an optimized ultra-short nacelle. Results show that nacelle geometry and the use of chevrons significantly influence drag, pressure recovery, temperature distribution, and fuel efficiency. The long nacelle with chevrons achieved the lowest drag coefficient (Cd = 0.0508), reduced temperature (200 K), and improved fuel performance (10.13% block fuel reduction), but its practicality is limited by added weight and cost.

An optimized ultra-short nacelle was developed via CFD simulations and hybrid optimization (NSGA-II with fmincon). Despite its compact size, it outperformed previous designs, achieving a lower drag coefficient (Cd = 0.0248) and reducing block fuel consumption by 80.13%. The broader chevron enhanced wake flow stability and reduced thermal hotspots. This configuration supports sustainability goals (SDGs 7, 8, 9, and 13), demonstrating the potential of intelligent nacelle design for greener aviation.

Future work should incorporate real-world nacelle design data and experimental validation to improve accuracy and practical applicability.

Author Contributions: The research study was carried out successfully with contributions from all authors.

Conflicts of Interest: The authors declare no conflict of interest.

References

Daggett, D. L., Kawai, R., & Friedman, D. (2003, December). *Blended wing body systems studies: Boundary layer ingestion inlets with active flow control* (NASA CR-2003-212670). National Aeronautics and Space Administration. Retrieved April 13, 2024 from https://ntrs.nasa.gov/api/citations/20040011052/downloads/20040011052.pdf.

Edwards, J. (2000). Thermal challenges in jet engines: An overview. *Journal of Propulsion and Power, 16*(1), 112–119. https://doi.org/10.2514/2.5550.

European Union Aviation Safety Agency. (2020a). CS-25.1191: Fire protection in engine compartments**.** *European Union Aviation Safety Agency*. Retrieved January 21, 2025 from https://www.easa.europa.eu.

European Union Aviation Safety Agency. (2020b). Certification specifications for engines (CS-E): Airflow and pressure recovery standards. *European Union Aviation Safety Agency*. Retrieved January 21, 2025 from https://www.easa.europa.eu.

Fischer, A. (2006). Thermal management systems for high-performance aircraft. *Aerospace Systems and Technology, 22*(5), 341–356.

Foudad, M., Sanchez-Gomez, E., Rochoux, M., Jaravel, T., & Terray, L. (2022, May). Present climate characterization and future changes in Clear-Air Turbulence (CAT) over the northern hemisphere. In *EGU General Assembly*.

General Electric Company. (2023). *Type certificate data sheet: GE9X-105B1A, GE9X-105B1A1, GE9X-105B1A2, GE9X-105B1A3* (Rev. 3). U.S. Federal Aviation Administration.

Jawahar, M., Sharen, H., & Gandomi, A. H. (2022). ALNett: A cluster layer deep convolutional neural network for acute lymphoblastic leukemia classification. *Computers in Biology and Medicine*, *148*, 105894.

Millot, G., Scholz, O., Ouhamou, S., Becquet, M., & Magnabal, S. (2020). Development of a 3D CFD aerodynamic optimization tool and application to engine air intake design," in *Proceedings of the 53rd 3AF International Conference on Applied Aerodynamics*, Salon de Provence, France, Mar. 26–28, 2018.

Nikolaidis, T., Jafari, S., Bosak, D., & Pilidis, P. (2020). Exchange rate analysis for ultra high bypass ratio geared turbofan engines. *Applied Sciences, 10*(21), 7945. https://doi.org/10.3390/app10217945.

Prosser, M. C., Williams, P. D., Marlton, G. J., & Harrison, R. G. (2023). Evidence for large increases in clear-air turbulence over the past four decades. *Geophysical Research Letters, 50*, e2023GL103814. https://doi.org/10.1029/2023GL103814.

Robinson, M., MacManus, D. G., Christie, R., Sheaf, C., & Grech, N. (2020). Nacelle design for ultra-high bypass ratio engines with CFD based optimisation. *Aerospace Science and Technology, 113*, Article 106191. https://doi.org/10.1016/j.ast.2020.106191.

Schuster, M., & Haag, A. (2022). Advancements in jet engine technologies: Balancing performance and efficiency. *Journal of Aerospace Engineering, 35*(4), 445–460.

Silva, V. T., Lundbladh, A., Petit, O., & Xisto, C. (2022). Multipoint aerodynamic design of ultrashort nacelles for ultrahigh-bypass-ratio engines. *Journal of Propulsion and Power*, *38*(4), 541-558.

Tam, C. K. W., & Parrish, S. A. (2015). Noise of high-performance aircraft at afterburner. *Journal of Sound and Vibration, 352*, 103–128.

Tejero, F., Robinson, M., MacManus, D. G., & Sheaf, C. (2019). Multi-objective optimisation of short nacelles for high bypass ratio engines. *Aerospace Science and Technology, 91*, 410–421.

Tomita, J. T., Bringhenti, C., Pozzani, D., Barbosa, J. R., de Jesus, A. B., de Almeida, O., & Oliveira, G. L. (2005, November 6–11). Overview on nacelle design. In *Proceedings of COBEM 2005, 18th International Congress of Mechanical Engineering, Ouro Preto, MG, Brazil*. ABCM.

Wernet, M. P., & Bridges, J. E. (2021). *Characterization of chevron nozzle performance* (NASA/TM-20210020164). National Aeronautics and Space Administration. Retrieved March 3, 2025 from https://ntrs.nasa.gov/citations/20210020164.